Available online at www.sciencedirect.com

ScienceDirect

Ceramics International 40 (2014) 1431–1438

CERAMICS INTERNATIONAL

www.elsevier.com/locate/ceramint

Analysis of water leaching and transition processes in zirconium oxychloride octahydrate production

Ran Liu[a,b,c], Jingkui Qu[b,c], Jing Song[b,c], Tao Qi[b,c], Ailing Du[a,*]

[a]School of Chemistry and Chemical Engineering, Shandong University, Jinan 250061, China
[b]National Engineering Laboratory for Hydrometallurgical Cleaner Production Technology, Beijing 100190, China
[c]Key Laboratory of Green Process and Engineering, Institute of Process Engineering, Chinese Academy of Sciences, Beijing 100190, China

Received 18 June 2013; received in revised form 4 July 2013; accepted 4 July 2013
Available online 16 July 2013

Abstract

The water leaching and transition process in manufacturing zirconium oxychloride octahydrate was examined. Results from X-ray diffraction (XRD) and Fourier-transform infrared (FT-IR) spectra showed that most of the soluble sodium silicate was dissolved and the residue hydrolyzed into H_2SiO_3 during the water leaching process. In addition, Na^+ from sodium zirconate ($NaZrO_3$) in the interlayer was removed during the first and second water leaching and the in-host layer was distinguished in the third water leaching. This process resulted in the hydrolysis of $NaZrO_3$ into $ZrO(OH)_2$. Results from the scanning electron microscopy (SEM), FT-IR spectra, nuclear magnetic resonance (NMR) and XRD of the transition process showed the main reaction and properties of the products at different pH values. Na_2ZrSiO_5 reacted with HCl at pH = 7, producing $ZrO(OH)_2 \cdot SiO_2$ and NaCl. $ZrO(OH)_2 \cdot SiO_2$ partially reacted with HCl, forming $ZrOCl_2$ and H_2SiO_3 with a decrease in pH.

Keywords: Zirconium oxychloride; Water leaching; Transition

1. Introduction

Zirconium has attracted considerable attention as a material for high-tech industrial applications because of its excellent mechanical, thermal, electrical, chemical, and optical properties. This element is widely used in ceramic production and nuclear reactors to clad fuel rods. Zirconium is also used to remove residual gases in electron tubes as well as to fabricate pumps, valves and heat exchangers [1–3]. Zirconium oxychloride octahydrate ($ZrOCl_2 \cdot 8H_2O$), an important basic chemical product, is the main raw material for zirconium-based chemicals, such as zirconium oxide, zirconium sulfate, and zirconium carbonate. According to the survey conducted by the China Nonferrous Metals Industry Association, China ranked first in $ZrOCl_2 \cdot 8H_2O$ production because it produced more than 200,000 t of $ZrOCl_2 \cdot 8H_2O$ in 2011. Alkali fusion of zircon sand concentrate, the key method for producing $ZrOCl_2 \cdot 8H_2O$, is highly efficient and can be used for large-scale production, compared with the chloride and lime sintering method. The alkali fusion technology is shown in Fig. 1 [4–6].

During alkali fusion, zircon is sintered thoroughly with sodium hydroxide (NaOH) at 750 °C, according to the following reactions [7–9]:

$$ZrSiO_4 + 2NaOH \rightarrow Na_2ZrSiO_5 + H_2O \quad (1)$$

$$ZrSiO_4 + 4NaOH \rightarrow Na_2ZrO_3 + Na_2SiO_3 + 2H_2O \quad (2)$$

$$ZrSiO_4 + 6NaOH \rightarrow Na_2ZrO_3 + Na_4SiO_4 + 3H_2O \quad (3)$$

Water leaching separates sodium zirconate (Na_2ZrO_3), sodium metasilicate (Na_2SiO_3), and sodium orthosilicate (Na_4SiO_4) formed during the alkaline melting, which is critical for silicon removal in the whole line. Na_2SiO_3, Na_4SiO_4 and unreacted NaOH are supposed to be soluble in water, whereas Na_2ZrO_3 should be hydrolyzed, remaining in the water insoluble residue. During the water leaching, a certain amount of zirconium is entrained in the silicon slag and discharged. If optimum silicon removal is performed, we can reduce the amount of silicon slag and the corresponding zirconium entrained can be reduced. This process will reduce the production cost and improve the

*Corresponding author. Tel./fax: +86 13678819446.
E-mail address: duailing56@163.com (A. Du).

0272-8842/$ - see front matter © 2013 Elsevier Ltd and Techna Group S.r.l. All rights reserved.
http://dx.doi.org/10.1016/j.ceramint.2013.07.026

zirconium extraction rate. Therefore, investigating the water leaching process is necessary.

Transition is performed not only to remove Na^+ from the material, but also influence the acid solution and flocculation process. However, its mechanism remains unclear; as a result denatrium is difficult to achieve. Thus, the transformation process is not performed and Na^+ remains in $ZrOCl_2 \cdot 8H_2O$. However, if the transition process is extensively studied, Na^+ removal and the quality of $ZrOCl_2 \cdot 8H_2O$ can be greatly enhanced.

Studies on the alkali fusion of zircon sand concentrate with NaOH have been conducted. However, the mechanism of the water leaching and transition technique has not been analyzed. To the best of our knowledge, the structural characterization of silicon and zirconium using X-ray diffraction (XRD), Fourier-transform infrared (FT-IR) spectra, scanning electron microscopy (SEM), and nuclear magnetic resonance (NMR) has not been reported. With the use of these techniques, the present study explores the relationship between the preparation conditions and properties of the materials. The mechanism and several key techniques of the water leaching and transformation processes are discussed in detail. Results from this study are anticipated to be beneficial in the understanding of $ZrOCl_2 \cdot 8H_2O$ production through alkali fusion.

2. Experimental procedures

2.1. Materials

The fused mass was provided by Jiangxi Jing'an Hi-technology Co. Ltd. The chemical composition of the sample is shown in Table 1, and results from the XRD analysis are presented in Fig. 2a. The samples primarily comprised Na_2ZrO_3 and Na_2SiO_3.

2.2. Analyses and measurements

The concentrations of Na_2O, SiO_2 and ZrO_2 in the aqueous solution were analyzed using inductively coupled plasma atomic emission spectra (ICP-AES) (IRIS/AP, Thermo Electron Corporation). Hydrogen and nitrogen in the xerogel were determined using a Perkin-Elmer Series II CHNS/O Analyzer 2400 (USA).

The physical structure was evaluated using an X-ray diffractometer (D/max-RB, Rigaku, Japan), with the following conditions: 40-kV CuKα radiation with a graphite monochromator, and 40 mA electric current. The patterns were obtained within a 5–90° 2θ angular interval with 0.05° step and 1 s of counting time.

The chemical structure was evaluated by FT-IR spectra (Perkin-Elmer spectrophotometer). The samples were prepared by mixing the materials and KBr in a proportion 1:200(w/w). For all spectra, eight scans were accumulated with a 4 cm^{-1} resolution.

The SEM micrographs of the solid particles were taken using a scanning electron microscope (JSM-35CF, Japan Electron Optics Laboratory Co., Ltd.).

A Bruker Avance 400 (9.4 Telsa) operating at a frequency of 79.5 MHz for the ^{29}Si nucleus was utilized to collect the NMR spectra. A standard double-air-bearing cross polarization–magic angle spinning (CP/MAS) probe was used. Ground samples were loaded into 7 mm fused zirconia rotors, sealed with Kel-F™ caps, spun at a magic angle with a spinning rate of 5 kHz at a delay time of 5 s. The observed signals were quantified by directly comparing the areas of the peaks. All chemical shifts were externally referenced to tetramethyl silicane.

Diffuse reflectance spectra of the samples were recorded on a UV-2000 spectrometer equipped with an integrating sphere, using $BaSO_4$ as a reference material.

2.3. General procedure

2.3.1. Water leaching process

All experiments were conducted in batch mode and three level countercurrent water leaching processes. The leaching experiments were conducted in a 2-L volume plastic cup. The fused mass (200 g) was mixed with deionized water (L/S=4:1) of 50 °C, via mechanical stirring at 300 rev/min for 30 min. Solid–liquid separation was subsequently achieved. Sodium, silicon and zirconium contents of the final washed residue were analyzed by ICP-AES.

2.3.2. Transition process

The water leaching product (500 g) was mixed with deionized water (1000 g) in a plastic cup and put in a water bath at 65 °C. The pH value was adjusted using HCl (5.5 mol/L) to 1, 3, or 7 under mechanical stirring at 300 rev/min. The sample precipitated at a stable pH after 40 min. Deionized water (1500 g) was added to the plastic cup with constant stirring for 5 min. The water was filtered, washed thoroughly with deionized water (2000 g), and analyzed.

Fig. 1. Technological process of $ZrOCl_2 \cdot 8H_2O$ production by alkali fusion.

Table 1
Chemical composition of the fused mass.

Component	Na_2O	ZrO_2	SiO_2	HfO_2	Cl	K_2O	TiO_2	Fe_2O_3
Content (ω, %)	51.28	28.05	16.99	0.715	1.363	0.356	0.213	0.208

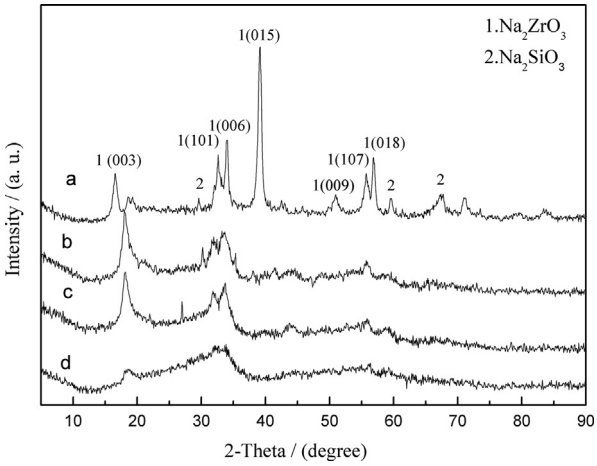

Fig. 2. XRD patterns of the water leaching technology: (a) the fused mass; (b) the first water leaching product; (c) the second water leaching product; (d) the third water leaching product.

3. Results

3.1. Analysis of the water leaching process

The content of the insoluble residue obtained from the water leaching process is shown in Table 2. The mechanism analysis is presented as follows.

3.1.1. XRD analysis

The crystallographic nature of the residue was investigated by XRD. The XRD peaks of Na_2ZrO_3 and Na_2SiO_3 gradually disappeared during the water leaching process (Fig. 2). No XRD peak of the two compounds was found in the third leaching product. Previous studies have indicated that cubic ZrO_2 is normally unstable at room temperature, unless Na is incorporated into the lattice [10–12]. The new peaks in the first and second leaching products were probably caused by the partial replacement of Na^+ by H^+, H_2O or H_3O^+ resulting in the decreased distances of the crystalline structure. The XRD results indicated that the unit cell *c* decreased from 16.3 Å of Na_2ZrO_3 to 14.7 Å of $ZrO(OH)_2$, which shifted the 003 crystal peak position to a high angle. Na^+ in the host layer was only removed during the third water leaching, which resulted in an amorphous material [13–15]. The water leaching material was thermally treated to explore the structure of the amorphous material. XRD results showed that the water leaching product dehydrated at 350 °C remained amorphous, suggesting that a crystalline was not formed (Fig. 3). The ZrO_2 crystal appeared at 500 °C. The formation of the water leaching product was observed clearly at 750 °C [16]. The products of different water leaching times at 750 °C are shown in Fig. 4. The main contents of the heat-treated water leaching product were ZrO_2, SiO_2 and Na_2ZrSiO_5.

3.1.2. FT-IR spectra analysis

The FT-IR spectra for the water leaching products are illustrated in Fig. 5. The results show that the broad band centered upon 3406 cm^{-1} has been caused by the atmospheric moisture retained by the KBr pellet and from the –OH groups in the material. The bands at 2368 and 2345 cm^{-1} may be related to the coordinated water caused by the "scissor" bending mode of the water molecule. The band may also be related to the atmospheric constituent CO_2 adsorbed on the xerogel because CO_2 interacted with terminal OH groups present on the partially dehydrated xerogel surface, yielding bicarbonate-like species, the O–C–O stretching bands of which are visible at 2360 cm^{-1} [17]. The bands observed at 1528 and 1367 cm^{-1} may be attributed to the bidentate carbonates formed by the "side-on" coordination of the atmospheric constituent of CO_2 on coordinatively unsaturated O^{2-}–Zr^{4+} pairs [18,19] from Na_2ZrO_3 hydrolyzation. The band at 970 cm^{-1} is associated with the Si–O–Zr bond, which is

Table 2
Chemical composition of the water leaching materials.

Component	SiO_2	Na_2O	ZrO_2
Content (*ω*, %)	6.77	7.049	57.169

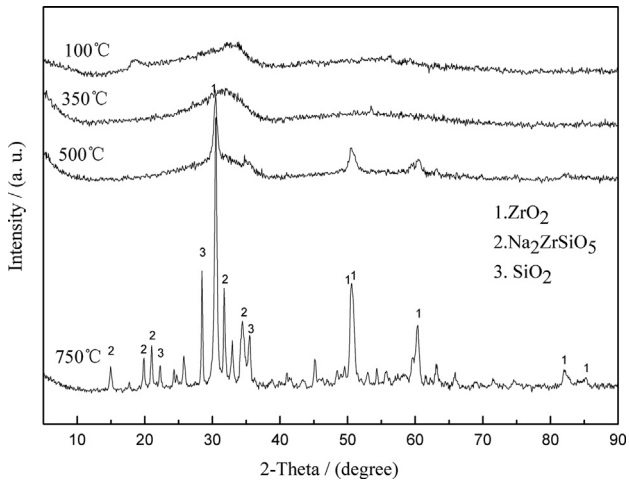

Fig. 3. XRD patterns of the water leaching products heat-treated at different temperatures.

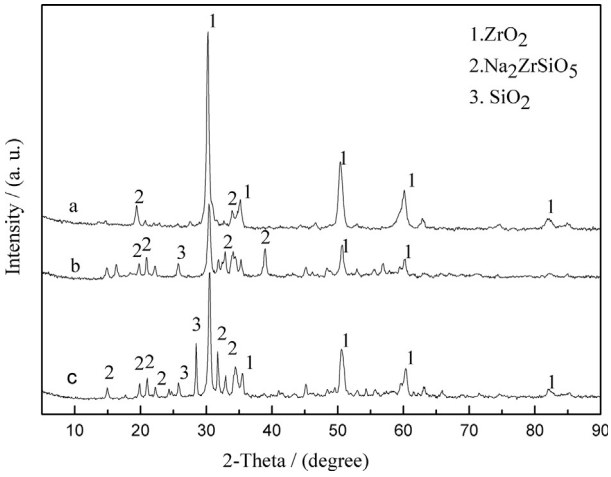

Fig. 4. XRD patterns of the water leaching products heat-treated at 750 °C: (a) the first water leaching product; (b) the second water leaching product; (c) the third water leaching product.

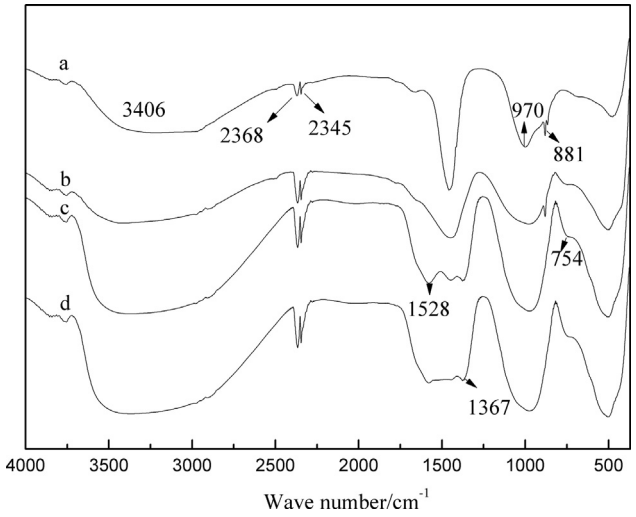

Fig. 5. FT-IR spectra of the water leaching technology: (a) the fused mass; (b) the first water leaching product; (c) the second water leaching product; (d) the third water leaching product.

believed to have resulted from a part of the zirconium incorporated into the silica network to form Si–O–Zr band [20]. Hence, the Si–O–Zr network formation confirms the existence of Na_2ZrSiO_5. The Si–O–Si symmetrical and bending vibration bands can be positioned at 754 cm^{-1}, indicating SiO_2 formation with low degree of polymerization [21]. The disappearance of the peak at 881 cm^{-1} indicates the absence of NaOH.

3.2. Analysis of transition process

The transition experiment at different pH values is shown in Table 3. The draft filtering time decreased as the pH value increased, and the sodium content satisfied the requirement at pH values lower than 5. The mechanism of the transition process was analyzed in the following experiment.

3.2.1. XRD analysis

The transition product was amorphous after drying at 100 °C. Thermal treatment was performed to explore the structure of the amorphous material. XRD results showed that the transition product dehydrated at 350 °C remained amorphous, suggesting that a crystalline was not formed (Fig. 6). The formation was clearly observed at 750 °C. The main contents of the heat-treated transition product were ZrO_2, SiO_2, or $ZrO_2 \cdot SiO_2 \cdot H_2O$.

3.2.2. FT-IR spectra analysis

The structural changes in the products observed through FT-IR spectra are shown in Fig. 7. The peak at 970 cm^{-1} shifted to 1030 cm^{-1} because of the disappearance of Na_2ZrSiO_5. This phenomenon is due to the replacement of Na^+ by H^+ or the formation of Si–O–Si bonds as a result of the Si–O–Zr vibration. The transition products at different pH values indicated that the bond energy increased with a decrease in pH (Fig. 8).

3.2.3. NMR analysis

The microstructure of the transition product was probed using the ^{29}Si CP/MAS NMR technique. The key to the nomenclature used in the present study to interpret the ^{29}Si CP/MAS NMR spectra is illustrated in Fig. 9. The chemical shift regions associated with these chemical structures are listed, for reference, in Table 4 [22]. The transition material at pH = 1 and pH = 3 showed typical resonances for silane-diols (Q^2), silanols (Q^3) and siloxanes (Q^4) (Fig. 10). In addition, the material at low pH showed a higher degree of polymerization than the material at a higher pH because of presence of more siloxanes (Q^4). The transition material at pH = 7 showed typical resonances for silanols (Q^3). This deduction is supported by the FT-IR spectra results which showed the existence of SiO_2. Based on the ^{29}Si CP/MAS NMR technique, we conclude that $Si(OSi)_4$ was formed at low pH values, which can be reflected as follows:

$$Na_2ZrSiO_5 + 2HCl \rightarrow ZrO(OH)_2 \cdot SiO_2 + 2NaCl (pH = 7) \quad (4)$$

Part of the $ZrO(OH)_2 \cdot SiO_2$ occurred through the following reaction with the addition of an acid:

$$ZrO(OH)_2 \cdot SiO_2 + 2HCl \rightarrow ZrOCl_2 + H_2SiO_3 + H_2O (pH = 1, pH = 3) \quad (5)$$

The analytical results are contradictory to those obtained from a previous study [23], which showed that

$$Na_2ZrSiO_5 + 2HCl \rightarrow ZrSiO_4 + 2NaCl + H_2O \ (HCl < 1.2\ M) \quad (6)$$

$$Na_2ZrSiO_5 + 4HCl \rightarrow ZrOCl_2 + H_2SiO_3 + 2NaCl + H_2O (HCl > 1.2\ M) \quad (7)$$

Reactions of (6) and (7) are valid for a pure substance, which was confirmed in our laboratory. However, pure Na_2ZrSiO_5 is different from Na_2ZrSiO_5 in water leaching material which will be proven in the following UV–vis diffuse reflectance spectra (UV–vis).

3.2.4. UV–vis analysis

UV–vis spectra were used to study the domain size of the material in Fig. 11. Two absorption edges were observed in zirconia, particularly at 250 and 347 nm. The low-energy (higher wavelength) step in zirconia is attributed to the $O^{2-} \rightarrow Zr^{4+}$ charge transfer transitions from O^{2-} in the low coordination sites on the surface of the small particles, whereas the step at higher energy is due to the direct band gap of the bulk tetragonal zirconia phase [24]. The water leaching product is amorphous as shown by XRD. Hence, only the 338 nm absorption is attributed to $ZrO_2 \cdot H_2O$. The absorption edge at 266 nm shifted from 286 nm in Fig. 11, which exhibited a "blue-shift" compared with the Na_2ZrSiO_5 determined by the decreasing particle size. The ratio of the number of surface atoms with respect to the total atomic number of a cluster or an ultrafine particle increased with a decrease in its dimension, and then its surface effect intensified [25]. This process facilitated the reaction of Na_2ZrSiO_5 in water leaching products and HCl at lower concentrations.

3.2.5. SEM analysis

SEM micrographs showed that Na_2ZrSiO_5 reacted with HCl at different pH values (Fig. 12). Floccular formation was observed at lower pH values, proving the formation of silica gel.

Table 3
Transition process at different pH values.

pH	Consumption of HC1 (mol)	Draft filtering time (min)	SiO_2 (%)	Na_2O (%)	ZrO_2 (%)
1	1.65	210	10.412	0.524	54.248
2	1.43	140	10.414	0. 243	58.041
3	1.386	60	10.784	0.0207	56.172
4	1.331	50	6.984	0.0365	58.69
5	1.21	45	9.033	0. 71	56.799
6	1.023	40	10.063	1.58	54.868
7	0.913	30	9.596	2.6	56.91

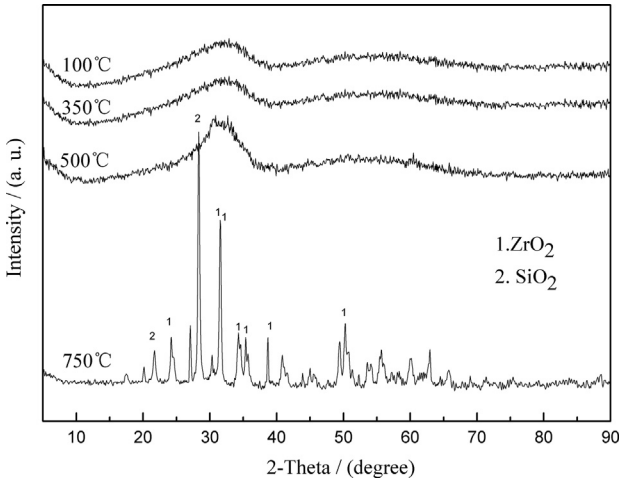

Fig. 6. XRD patterns of the transition products at pH = 3 heat-treated at different temperatures.

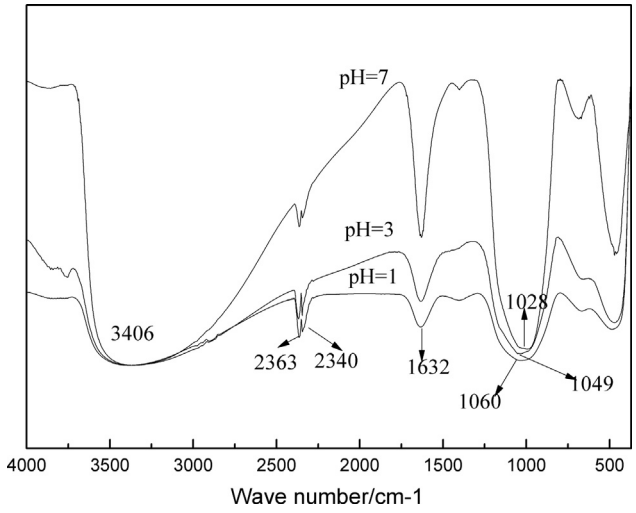

Fig. 8. FT-IR spectra of the transition products at different pH values.

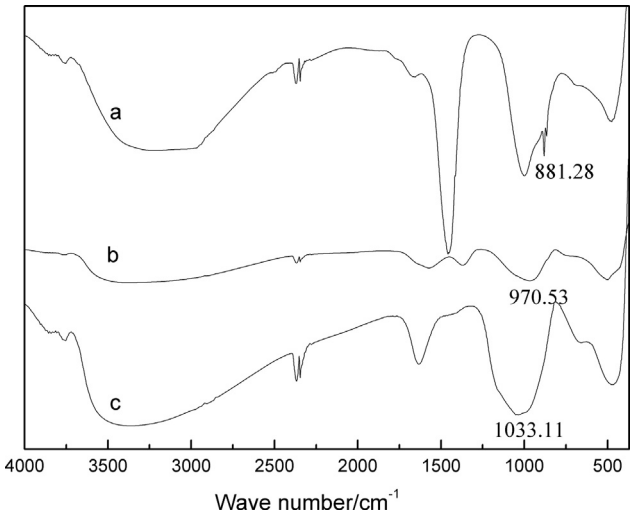

Fig. 7. FT-IR spectra of the water leaching and transition processes: (a) the fused mass; (b) water leaching products; (c) transition products.

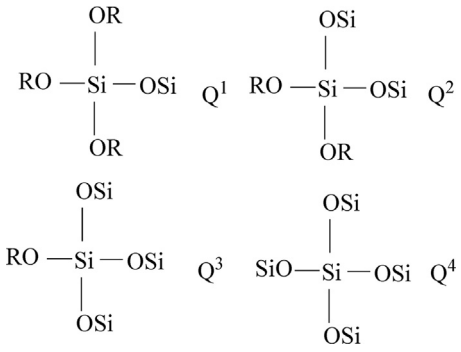

Fig. 9. Key structural features detected by ^{29}Si CP/MAS NMR.

4. Discussion

Disappearing of the peak of Na_2SiO_3 in Fig. 2 proves that most of those were dissolved. SiO_2 formed because of the hydrolyzed Na_2SiO_3 during the second leaching process. The chemical

Table 4
Chemical shift regions of the ^{29}Si CP/MAS NMR spectra.

Silica atom	Chemical shift (ppm)
Zero order	−70 to −72
First order	−77.5 to −80.7
Secondary linear chain	−88 to −90.5
Secondary link chain	−80 to −82.5
Third order	−92.6 to −98.5
Fourth order	−108 to dispersion

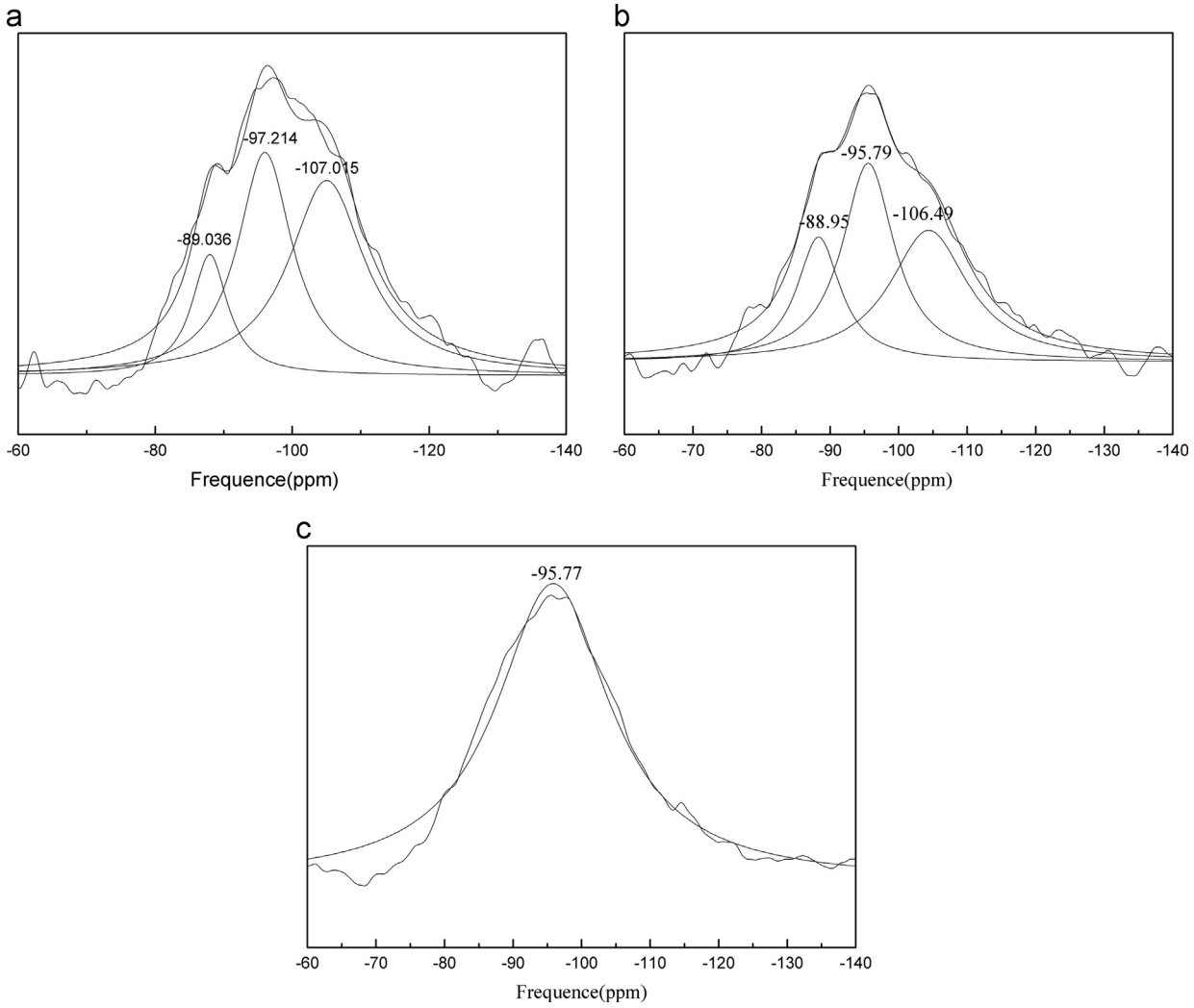

Fig. 10. ^{29}Si CP/MAS NMR spectra for the transition product at different pH values: (a) pH=1; (b) pH=3; (c) pH=7.

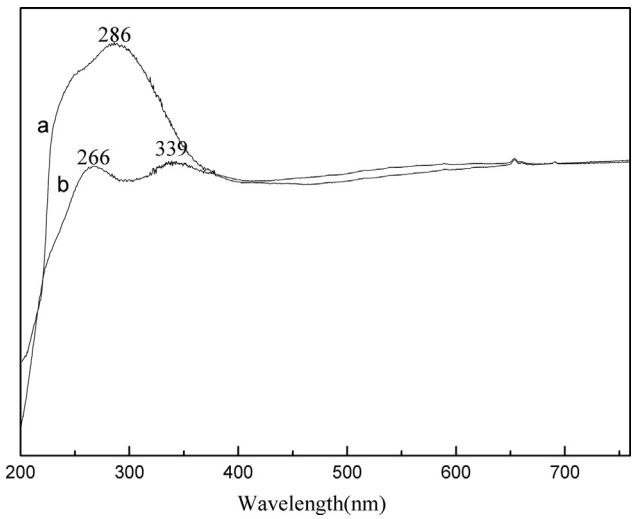

Fig. 11. Uv–vis spectra of the material.

composition of Na_2SiO_3 and Na_2SiO_4 can be expressed by the general formula: $mNa_2O \cdot nSiO_2$. The dissolution process starts with the dissolution of Na_2O, with only a small amount of dissolved SiO_2. Subsequently, the residual swelled silica gel was dissolved with only a small amount of the remaining alkali. Therefore, the dissolution of SiO_2 is actually composed of the hydration of sodium silicate with NaOH formation, followed by the dissolution of Na_2SiO_3 and dissociation. Finally, the residual SiO_2 is peptized by the strong alkaline solution. The concentration of OH^- ions increased considerably with the dilution of Na_2SiO_3 [26,27]. During the first leaching process, the alkaline concentration was approximately 3.4 mol/L, so $mNa_2O \cdot nSiO_2$ was dissolved with a small amount of Na_2SiO_3 residue. Then, alkaline concentration decreased, and the remaining Na_2SiO_3 began to hydrolyze into SiO_2. A large proportion of the silica in the aqueous solution of mono- and disilicate existed in colloidal form. However, the SiO_2 solutions contained complexes of mono- and disilicates, with an excess of SiO_2 or hydrated silica. Thus, the FT-IR spectra showed a low degree of polymerization at 754 cm^{-1}. With an increase in temperature (50 °C), both the Na_2O solution and the SiO_2 peptization also increased, which resulted in the significant increase in silicon dissolution rate.

Previous reports have shown that Na_2ZrO_3 can only be hydrolyzed when the alkalinity is lower than 0.25 mol/L

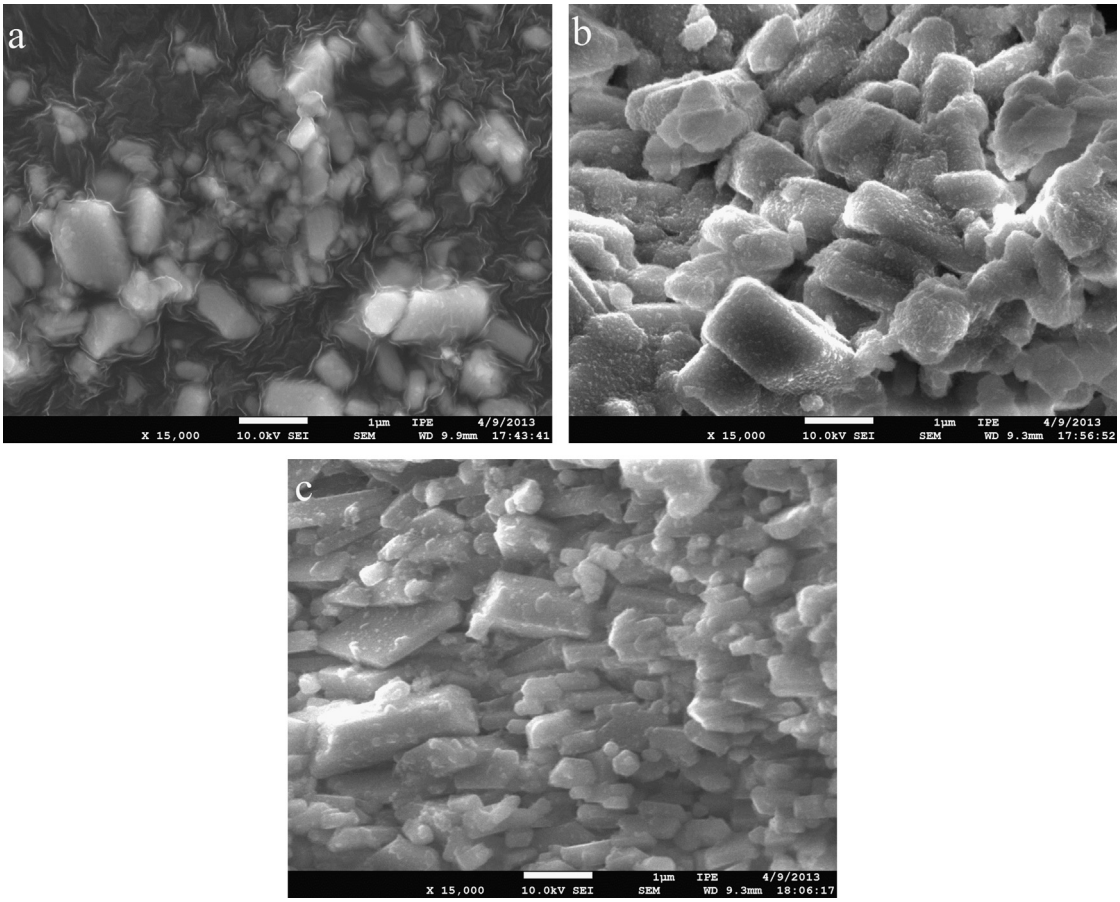

Fig. 12. SEM view of transition material: (a) pH=1; (b) pH=3; (c) pH=7.

[4]. The current study showed that certain hydrolysis of Na_2ZrO_3 occurs, and the alkalinities of one- and two-stage scrubbings were 3.4 and 1 mol/L, respectively. Na^+ in the interlayer was removed in the two water leaching processes. Na^+ in the host layer was distinguished only when the alkalinity was lower than 0.25 mol/L. $ZrO(OH)_2$ is amorphous. Hence, the crystal water detraction transpired at 130 °C, and the following decomposition reaction [Reaction (8)] occurred is at 340 °C. The crystal structure appeared at 750 °C, as shown in the XRD patterns [28].

$$ZrO(OH)_2 = ZrO_2\downarrow + H_2O$$

If the Na_2ZrO_3 hydrolysis is hindered, the remaining Na_2ZrO_3 would react with HCl in the subsequent step, which will decrease the amount of zircon. Thus, the water leaching process should ensure the hydrolysis of Na_2ZrO_3 through sufficient time. The $ZrO(OH)_2$ formed during the water leaching process did not change during the transition technique because almost no zirconium particle appeared in the filter liquor.

Na_2ZrSiO_5 existed in the entire water leaching line. Thermodynamic analysis showed that the following reaction occurred at 750 °C [29,30]:

$$ZrO_2 + Na_2SiO_3 \triangleq Na_2ZrSiO_5, \quad G > 0 \tag{9}$$

In addition, the alkali fusion was conducted at 750 °C. Thus, Na_2ZrSiO_5 was not generated during the heating of the watering material, but existed in the fused products, the XRD peak of which was covered by another peak and reacted with HCl in the transition procedure. The main reaction during transition was analyzed through XRD, FT-IR spectra, NMR, UV–vis, and SEM analyses. During leaching with a low HCl concentration (pH > 7), zircon lines appeared from the incomplete removal of Na_2ZrSiO_5. In this case, the HCl added was sufficient only to react with Na^+ in Na_2ZrSiO_5, forming NaCl according to Reaction (4). At HCl high concentrations (pH < 7), the $ZrO(OH)_2 \cdot SiO_2$ also disappeared gradually, which can be ascribed to the precipitation of both H_2SiO_3 and $ZrOCl_2$ in fine form. During transition process, Na^+ should be removed, and H_2SiO_3 formation should be minimized to decrease draft filtering time and keep the material stable. Thus, pH=3 should be chosen as the appropriate environment.

5. Conclusions

A series of characteristic analysis have been developed to resolve the challenges in the water leaching and transition technique of $ZrOCl_2 \cdot 8H_2O$ production by alkali fusion. The following conclusions can be drawn.

(1) Most of the Na_2SiO_3 was dissolved, and the residue was hydrolyzed into SiO_2. Na^+ of Na_2ZrO_3 in the interlayer was removed during the first and second water leaching and in host layer was distinguished in the third water leaching. This

process resulted in the hydrolysis of $NaZrO_3$ into $ZrO(OH)_2$. Na_2ZrSiO_5 remained unchanged.

(2) The reaction of Na_2ZrSiO_5 with HCl is considered as the main reaction. The materials formed during transition behaved differently from those precipitated under different pH values. Na_2ZrSiO_5 reacted with HCl at pH = 7, producing $ZrO(OH)_2 \cdot SiO_2$ and NaCl. $ZrO(OH)_2 \cdot SiO_2$ partially reacted with HCl, forming $ZrOCl_2$ and H_2SiO_3 with a decrease in pH. Thus, pH = 3 was chosen as the appropriate environment.

Acknowledgments

This work was supported by the Jiangxi Jing'an Hi-technology Co. Ltd.

References

[1] L.Z. Han, Development problem and prospect of zirconium chemicals in China, Rare Metals Letters 26 (2007) 17–19.
[2] B.K. Xiong, Z.H. Lin, X.M. Yang, Preparation and Application of Zirconia, Metallurgy Industry Press, Beijing, pp. 74–84.
[3] R.K. Biswas, M.A. Habib, A.K. Karmakar, M.R. Islam, A novel method for processing of Bangladeshi zircon: Part I: baking, and fusion with NaOH, Hydrometallurgy 103 (2010) 124–129.
[4] D.M. Jiang, L.J. Wang, X.K. Che, Preparation and Application of Zirconium, Oxychloride Metallurgy Industry Press, Beijing, pp. 34–45.
[5] N.Q. Minh, T. Takahashi, Science and Technology of Ceramin Fuel Cells, Elsevier, pp. 366–376.
[6] G. Singh, Chemistry of D-Block Elements, Discovery Publishing House, New Delhi, pp. 315–320.
[7] R. Stevens, Zirconia and Zirconia Ceramics, 2nd edn., Magnesium Elektron Ltd, Twickenham, UK, pp. 223–230.
[8] Z. Li, Y. Huang, H. Yao, M. Yang, J. Chen, Preparation of zirconium oxychloride via alkali fusing of zirconium carbide, Chinese Journal of Rare Metals 30 (2006) 415–418.
[9] A. Manhique, Z. Kwela, W.W. Focke, De wet process for the benification of zircon: optimization of the alkali fusion step, Industrial and Engineering Chemistry 42 (2003) 777–783.
[10] H. Nishizawa, N. Yamasaki, K. Matsuoka, H. Mitsushio, Crystallization and transformation of zirconia under hydrothermal conditions, Journal of the American Ceramic Society 65 (1982) 343–346.
[11] A. Benedetti, G. Fagherazzi, F. Pinna, Preparation and structural characterization of ultrafine zirconia powders, Journal of the American Ceramic Society 72 (1989) 467–469.
[12] A. Benedetti, G. Fagherazzi, F. Pinna, S. Polizzi, Structural properties of ultra-fine zirconia powders obtained by precipitation methods, Journal of Materials Science 25 (1990) 1473–1478.
[13] G. Fagherazzi, P. Canton, A. Benedetti, F. Pinna, G. Mariotto, E. Zanghellini, Rietveld analysis of the cubic crystal structure of Na-stabilized zirconia, Journal of Materials Research 12 (1997) 318–321.
[14] P. Canton, G. Fagherazzi, R. Frattini, P. Riello, Stabilization of cubic Na-modified ZrO_2: a neutron diffraction study, Journal of Applied Crystallography 32 (1999) 475–480.
[15] H. Nafe, N. Karpukhina, Na-modified cubic zirconia—link between sodium zirconate and zirconia in the Na_2O–ZrO_2 phase diagram, Journal of the American Ceramic Society 90 (2007) 1597–1602.
[16] V.I. Babushkin, G.M. Matveyev, O.P. Mchedlov-Petrossyan, Thermodynamics of Silicates, 4th Edn., Springer-Verlag, Berlin, pp. 276–428.
[17] G.Y Guo, Y.L. Chen, Preparation and characterization of a novel zirconia precursor, Ceramics International 30 (2004) 469–475.
[18] Y. Yu, X.P. Wang, Y.Z. Cao, X.F. Hu, Study on the structure and properties of ZrO_2 buffer layers on stainless steel by XRD, IR and AES, Applied Surface Science 172 (2001) 260–264.
[19] V. Bolis, G. Magnacca, G. Ceratto, C. Morterra, Microcalorimetric and IR-spectroscopic study of the room temperature adsorption of CO_2 on pure and sulphated t-ZrO_2, Thermochimica Acta 379 (2001) 147–161.
[20] R. Chen, X.Q. Song, Preparation of nanostructural ZrO_2-coated SiO_2 particles by layer-by-layer assembly technique, Journal of the Chinese Chemical Society 51 (2004) 945–948.
[21] Y. Ivanova, Nanostructured hybrid materials as precursors for synthesis of nanocoposites in Si–O–C–N–Zr system, Thin Solid Films 515 (2006) 271–278.
[22] Lu Chen, Ji Dengshen, Zhu Cunxi, Determination and research on constituents of water glass, Journal of Shanghai Jiaotong University 31 (1997) 86–89.
[23] K.A. El Barawy, S.Z. El Tawil, A.A. Francis, Alkali fusion of zircon sand, Mineral Processing and Extractive Metallurgy Review 109 (2000) 49–56.
[24] S.H. Liu, S. Jaenicke, G.K. Chuah, Hydrous zirconia as a selective catalyst for the meerwein–ponndorf–verley reduction of cinnamaldehyde, Journal of Catalysis 206 (2002) 321–330.
[25] M. Anpo, T. Shima, S. Kodama, et al., Photocatalytic hydrogenation of propyne with water on small-particle titania: size quantization effects and reaction intermediates, Journal of Physics and Chemistry 91 (1987) 4305–4310.
[26] S.M. Bulatovic, Handbook of Flotation Reagents: Chemistry, Theory and Practice: Volume 1: Flotation of Sulfide Ores, Elsevier, Oxford , pp. 65–68.
[27] Z.C. Chen, Research for washing and eliminating of silica technology in manufacturing of zirconium oxchloride, Gongdong Chemical Engineering 9 (2004) 12–13.
[28] M.Angeles Diaz-Diez, Antonio Macias-Garcia, Theoretical study of the molecular structure for zirconium complexes, Ceramics International 29 (2003) 471–475.
[29] R. Subasri, T. Mathews, K. Swaminathan, O.M. Sreedharan, Thermodynamic stability of Na_2ZrO_3 using the solid electrolyte galvanic cell technique, Journal of Nuclear Materials 300 (2002) 237–241.
[30] P.L. Brown, Chemical Thermodynamics of Zirconium, Elsevier, Amsterdam, pp. 220–230.